36th European Rotorcraft Forum, Paris, France, September 7-9, 2010
Paper No. 147

Flow Field Characterization and Interactional Aerodynamics Analysis on a Full Helicopter Model

Fabrizio De Gregorio[1], Davide Cinquegrana[2]

[1] SIAE/IWTU laboratory, Italian Aerospace Research centre (CIRA), via Maiorise, 81043 Capua, Italy, email:f.degregorio@cira.it
[2] DIAM/SUN, Seconda Università di Napoli, via Roma 29, 81031, Aversa, Italy.

Abstract

The flow field around a helicopter is characterised by its inherent complexity including effects of fluid-structure interference, shock-boundary layer interaction, and dynamic stall. Since the advancement of computational fluid dynamics and computing capabilities has led to an increasing demand for experimental validation data, a comprehensive wind tunnel test of a fully equipped and motorized generic medium size transport helicopter was conducted in the framework of the GOAHEAD project.
In this paper the test campaign results in terms of three-components velocity field and fluid-structures interaction are discussed. The effect of the interaction between the main rotor wake and the fuselage for cruise/tail shake conditions was investigated, analysing the flow characteristics downstream the rotor hub and the rear hatch for the case of isolated fuselage and full equipped model. The results indicated a sensible increment of the intensity of the vortices shedding form the lower part of the fuselage and a strong influence of the main rotor in the upper region.
The main rotor fuselage interaction effects are further discussed taking into account the global effect in terms of static and dynamic loads and static and dynamic pressure distributions measured on the fuselage model.
Furthermore, the pitch up phenomenon was considered, detecting the blade tip vortices impacting on the horizontal tail plane, and measuring the effects on the horizontal tail plane in terms of vertical loads, pressure distribution and integral sectional forces and finally the effect on the full fuselage loads. For high speed forward flight the shock wave forming on the advancing blade was investigated, measuring the location on the blade chord and the its intensity.

Nomenclature

a_∞	Free-stream speed of sound [m/s]
α_s	Shaft angle [°]
C_x	Fuselage force coefficients in X-direction [-]
C_{mx}	Fuselage pitching moment coefficient [-]
C_M	Horizontal stabilizer pressure sectional load pitching moments [-]
C_N	Horizontal stabilizer pressure sectional vertical load [-]
C_T	Horizontal stabilizer pressure sectional horizontal load [-]
C_p	Pressure coefficient = $2(p-p_\infty)/(\rho_\infty U_\infty^2)$ [-]
C_z	Fuselage force coefficients in Z-direction [-]
r	Radial position along rotor blade [m]
R	Rotor radius [m]
M_{WT}	Wind tunnel Mach number
M_{tipTR}	Tail rotor tip Mach number
M_{MR}	Rotor tip Mach number
Ω_{MR}	Main rotor rotational speed [rpm]
Ω_{TR}	Tail rotor rotational speed [rpm]
μ	Advance ratio $=V_{tip}/ U_\infty$ [-]
p	Pressure [N/m^2]
p_∞	Free-stream pressure [N/m^2]
U_∞	Free-stream velocity [m/s]
θ_F	Fuselage pitch attitude [°]
ρ_∞	Free-stream density [kg/m^3]
Ψ_{MR}	Main rotor azimuth angle [°]

1. Introduction

Nowadays, the characterization of the flow field around a fully equipped helicopter still remains a challenging task. The complexity of the helicopter aerodynamics is characterized by unsteady flow-structure interaction, in particular, between the main rotor wake and the rear of the fuselage as well as the tail rotor. Phenomena know as *pitch up* and *tail shake* seriously interfere with handling quality and structural safety of the machine. Furthermore, phenomena such as shock wave-boundary layer interaction or dynamic stall occurring respectively on the advancing blade

under-high speed flight and on the retreating blade, under-high speed/high loaded rotor conditions, greatly affect the rotor performance and the structural integrity of the main rotor.

During the past decade considerable progress has been made in developing and advancing experimental aerodynamic prediction capabilities for isolated helicopter components. The isolated main rotor downwash structure, for example, has been investigated mainly by means of optical methods under hover conditions [1,2,3] or low-speed forward flight coupling main rotor with fuselage model [4, 5, 6].

Today, cutting edge computational fluid mechanics (CFD) tools are capable of predicting the viscous flow around rotor-fuselage configurations advancing towards complete helicopters. However, a detailed experimental validation data base to qualify methods and industrial design tools is still lacking.

In order to fill this gap, a comprehensive experimental database for validation purposes was created within the European Union funded project GOAHEAD [7] with special emphasis on unsteady viscous flow phenomena like flow separation, transition and including rotor dynamics.

In spring 2008, an extensive wind tunnel test campaign was performed in the Large Low-speed Facility of the German-Dutch wind tunnels (DNW-LLF) using a Mach-scaled model of a modern medium size transport helicopter. The model comprised the complete helicopter fuselage integrated with a motorised four blades main rotor and with a two blades tail rotor (Figure 1). The experiments foresaw measurements of the: global forces of the main rotor and fuselage, normal force and bending moments acting on the horizontal stabilizer, axial force and torque of the tail rotor, steady and unsteady pressures, boundary layer transition detection, stream lines. Furthermore the position of flow separation, the velocity fields in proximity of the model fuselage and on the upper surface of the advancing and retreating rotor blades, the vortex trajectories and the elastic deformations of the main rotor blades were investigated [8].

Two model configurations were investigated by means of planar three-component particle image velocimetry (PIV). Both the isolated fuselage with rotating hub mounting stubs instead of blades and the fully equipped model were considered. A variety of flight conditions and flow field regions were investigated within and beyond the generic helicopter mission envelope. Besides cruise flight conditions, pitch up, tail shake and high speed phenomena were addressed. Also dynamic stall was investigated but is separately discussed in [9].

In this paper the test campaign results in terms of three-components velocity field and interactional aerodynamic effect are discussed. The effect of the interaction between the main rotor wake and the fuselage for cruise/tail shake conditions was investigated, analysing the flow characteristics downstream the rotor hub and the rear hatch for the case of isolated fuselage and full equipped model. The main rotor fuselage interactional effects are further discussed taking into account the global effect in terms of static and dynamic loads and static and dynamic pressure distributions measured on the fuselage model. Furthermore, the pitch up phenomenon was considered, detecting the blade tip vortices impacting on the horizontal tail plane, and measuring the effects on the horizontal tail plane in terms of vertical loads, pressure distribution and integral sectional forces and finally the effect on the full fuselage loads. For high speed forward flight the shock wave forming on the advancing blade was investigated, measuring the location on the blade chord and the its intensity.

2. Experimental Configuration

2.1. LLF-DNW wind tunnel

The tests were carried out in the Large Low-speed Facility (LLF) of the German-Dutch wind tunnels (DNW). The LLF is a closed loop industrial wind tunnel for the low-speed domain with a 8 x 6 m^2 closed test section operated at a maximum Mach number of M_{WT}=0.34. The tests were performed at M_{WT}=0.059 for the pitch up condition, at M_{WT}=0.209 for cruise and tail shake conditions and at M_{WT}=0.259 for the high speed condition.

2.2. Model Description

The model was composed of a NH90 fuselage scaled by a factor of 1:3.88 (Figure 2). The fuselage was equipped with 300 steady pressure taps, 38 hot films sensors and 130 unsteady pressure transducers. The fuselage was integrated with the ONERA 7AD main rotor including the rotor hub. The four-bladed rotor had a radius of 2.1 m rotating clockwisely (as seen from above). The entire test campaign was performed at constant main rotor speed of Ω_{MR}=956 rpm, corresponding to a blade tip Mach number of M_{MR} =0.617. The blades were instrumented with 118 dynamic pressure transducers for pressure distribution measurements at multiple span wise positions and with 40 hot film sensors for transition localization. The rotor shaft was inclined by α_s=-5° with respect the fuselage vertical axis.

A scaled two-bladed MBB Bo105 tail rotor with a radius of 0.383m and a S102 airfoil was used. The tail rotor was equipped with 36 dynamic pressure sensors. The rotational speed of the tail rotor was kept constant throughout the tests at five times the main rotor speed Ω_{TR}=4780 rpm corresponding to M_{tipTR}=0.563. Furthermore, static and dynamic loads of the main and tail rotor, of the fuselage, and of the horizontal

stabilizer were recorded by means of strain gauge and piezoelectric balances.

2.3. PIV Instrumentations

For the measurements five double cavities Nd-Yag lasers with pulse energies of 280 mJ per pulse were used in connection with four 4Mpx cameras installed by motorized Scheimpflug adapters. High quality lenses with 180mm and 200mm focal length and f-numbers of 2.8 and 2 respectively were used. The data acquisition was synchronized with the main rotor by means of a one-per-revolution signal and a phase shifter enabling the adjustment of the phase-angle of the main rotor Ψ_{MR}. Di-Ethyl-Hexyl-Sebacat (DEHS) particles atomized by 64 Laskin nozzle particle generators were used as flow tracers. The particles were distributed through a rake mounted in the settling chamber of the wind tunnel. The rake was remotely traversed to guide the homogeneous stream of tracers to the region of interest. The mean particle diameter was below 1 μm as confirmed by previous tests.

2.4. Flow Field Measurement Regions

The flow field measurement locations are indicated in Figure 3. The PIV measurements involved two different span wise locations on the advancing rotor blade (Ψ_{MR}=90°, black regions) at r/R=0.85 and 0.95 for high speed case (M_{WT}=0.259) in order to detect the forming shock wave.

The cross flow region downstream from the rotor hub (red regions) and downstream from the fuselage hatch (grey regions) under cruise and tail shake conditions (M_{WT}=0.209) were acquired. The vertical region above the horizontal stabilizer (green region) was considered with regard to the pitch up phenomenon (M_{WT}=0.059). In order to evaluate the interference between the main rotor and the fuselage, the cruise and tail shake conditions were recorded for the isolated fuselage and for the fully equipped model.

The PIV measurements were characterised by a spatial resolution varying from 1 to 3.6 mm, and the relative measurement error was estimated in the range from 0.09% to 3% of the maximum in plane velocity.

For each test condition at least 150 instantaneous velocity fields were acquired. The phase locked ensemble average velocity fields were analysed as well as all the instantaneous velocity fields. The vortex detection and characterization evaluating the main magnitudes as vorticity, circulation tangential and radial velocity components were carried out.

A full description of the different adopted experimental set ups, PIV data post processing and accuracy estimation is described in [13].

3. Results

3.1. Cruise/Tail shake

Tail shake is an aerodynamic phenomenon resulting from the interaction of rotor hub wake with the tail boom and the vertical tail invoking low frequency vibration, impacting on fatigue cycles of the vertical stabilizer and the tail rotor [11].

The analysis of the dynamic pressure and load data on the tail plane indicated that the selected flight cruise conditions coincided with tail shake. The test were performed at an incident Mach number of M_{WT}=0.209 and a fuselage incidence of θ_F =-2.5°. Nine parallel planes were measured starting from the zone immediately downstream the engine exhausts down to the vertical tail plane. The flow field was acquired for five different azimuth angles (Ψ_{MR} =0°, 22.5°, 45°, 67.5° and 90°). This region is characterised by highly unsteady flow due to separation starting form engine exhausts, the rotor hub wake and the main rotor blade. Unfortunately, during these measurements a malfunctioning of the acquisition system occurred (especially for the isolated fuselage model configuration) which caused the loss of most of the instantaneous velocity fields preventing a comparison between the two model configurations.

The velocity magnitude and the calculated stream lines for Ψ_{MR} =0° clearly indicated the presence of two major counter rotating vortices emerging from the fuselage exhausts (Figure 4). Investigating the out of plane vorticity coloured map, the two major counter rotating vortices (indicated by A and B in Figure 5) were clearly visible, along with a secondary pair of counter rotating vortices (indicated by C and D on the bottom of Figure 5) detaching from the tail boom. At Ψ_{MR} =45° an outstretched zone of high vorticity (indicated by E in Figure 5) indicated the presence of shear layer or the cut of a vortex parallel to the measurement plane. The vorticity strip was encountered on all the parallel measurement planes for some rotor azimuth angles (Ψ_{MR} =22.5°, Ψ_{MR} =45° and Ψ_{MR} =67.5°), following a slightly descendent path from the top right to the left of the flow region as the azimuth angle increased (Figure 6). Analogous the vorticity strip was detected for Ψ_{MR}=45° on all the cross flow planes. The vorticity strip followed a path from the left top to the middle top of the PIV image as the plane of measurement was moved from the region immediately downstream the fuselage exhaust toward the vertical tail plane (Figure 7).

The vorticity strip was attributed to the tip vortices shedding from the main rotor blades and crossing the measurement planes.

The lower fuselage zone was investigated in ten parallel planes at Ψ_{MR} =0°. The region downstream from the fuselage hatch was characterized by two

counter rotating vortices shedding from the fuselage (Figure 8).
The mean velocity components were measured for the two model configurations (Figure 10). The full model wake was characterized by a growth of the cross velocity component (v) and by a decrement of the vertical and axial velocity components (u and w) as consequence of the main rotor induced velocity. The rise of the momentum loss corresponded to a growth of the fuselage drag.
Analogous the path of the counter rotating vortices was deviated moving toward starboard and below respect the case of isolated fuselage (Figure 9).
The effect of the main rotor wake behaved on the vortex characteristics with a substantial increment of the strength of the vortices. The vortices maximum tangential velocity increased of about 75 % and the peak of vorticity presented an increment varying from 75% to 350% (Figure 11). The vortex centre location was detected on the instantaneous velocity fields showing a concentrate distribution. The centres distribution was characterised by a standard deviation varying from a minimum of 3mm to a maximum of 40 mm.
All unsteady pressures on the fuselage were gathered for 150 main rotor revolutions with 2048 samples per main rotor revolution. The pressure time history (Figure 12) showed the effect of the main rotor on the fuselage pressure detecting the four blade passage and measuring higher mean pressure values. For the isolated fuselage model, the four revolution periodicity was also detected by the sensors invested by the wake shedding from the rotating hub but the signals showed considerably lower values (Figure 12 sensor K14).
The fuselage mean pressure coefficient distribution obtained by the fuselage static and dynamic pressure sensors showed the Main rotor/fuselage aerodynamic interaction. The main rotor induced higher pressure distribution on the nose and on the vertical tail plane leading edge (Figure 13). At the same time, the horizontal tail plane was characterised by an increment of the flow expansion on the lower surface (Figure 13) increasing the downward vertical load on the tail and consequently rising the fuselage pitching moment.
As consequence of the main rotor fuselage aerodynamic interaction the global loads on the fuselage presented an increment of the mean value of the Cx coefficient (higher fuselage drag), a decrement of the Cz coefficient (vertical drag) (Figure 14) and an increment of the pitching moment Cmy (Figure 15).

3.2. Pitch-up

Pitch up is a low speed aerodynamic interference phenomenon which occurs during transition from hover flight to medium cruise speed or viceversa [10, 12]. The main rotor flow impinges on the horizontal tail unit, resulting in pitching moment fluctuations constraining the handling quality.
The Pitch up phenomenon was initially investigated at M_{WT} =0.059 and fuselage incidence of θ_F =1.9° on the base of preliminary CFD calculations using the aeromechanical code HOST [14] and previous pressure and loads measurement on the horizontal stabiliser.
The main rotor azimuth angle was selected on the base of the presence in the measurement region of the main rotor blade tip vortex. The tip vortex was detected at Ψ_{MR} in the range between 56° and 85°.
The PIV measurements (Figure 16) clearly showed the tail plane fully immersed in the main rotor wake and the tip vortex passing far above. The vortex trajectory, with the horizontal tail plane position, is shown in Figure 17. The results indicated that the pitch up condition was not fully reached for the selected test condition. In order to get the tip vortex impacting on the tail plane the wind tunnel Mach number was decreased respectively down to M_{WT}=0.043 and M_{WT}=0.031 and the fuselage incidence varied to θ_F =-1.1°.
For M_{WT}=0.043, the tip vortices moved closer to the tail plane (Figure 18 and Figure 19) and impacted on the leading edge for M_{WT} =0.031 (Figure 20). Furthermore counter rotating vortices shedding by the lower surface were detected, indicating that the stabilizer was stalled as consequence of the main rotor induced vertical velocity.
The tip blade vortex path behavior (Figure 21) showed a larger dispersion in the vortex centre distribution for the case at Ma=0.031 due to the interference with the stabilizer leading edge. The vorticity distribution of the blade tip vortex for the different wind speed showed a substantial similar behavior.
The vertical loads on the horizontal tail plane were analysed for the test cases performed respectively at M_{WT} =0.059 and M_{WT} =0.031 (Figure 22). The test characterised by the vortices impinging directly on the tail plane (M_{WT} =0.031), showed a substantial increment of the amplitude of the oscillating signal respect the case at higher flight speed, whereas the mean value was almost unchanged. Analogous the data spectral analysis (Figure 23) showed that the case at M_{WT}=0.031 presented stronger peaks in concomitance of the main rotor frequencies (16, 32, and 64 Hz) and lower peak for the tail rotor frequency (159 Hz).
The balance data indicated for both test cases a behaviour characterized by a 10 revolution period, distinctive of the tail plane blade passing. This periodicity was not due to the effective loads acting on the tail plane but was induced by the vibration generated by the tail rotor motor as demonstrated hereinafter by the analysis of the pressure data. The pressure time history behaviour on the horizontal tail

plane indicated a considerable expansion characterized by four revolution period on the lower surface (Figure 24) whereas the pressure evolution on the upper surface was characterized by a weaker compression with 10 revolution period (Figure 25) being directly influenced by the tail plane. The pressure sectional load coefficients (C_N, C_T and C_M) obtained by the post processor [15] integrating the pressure values on the tail plane section and calculating the normal, tangential and pitching moment components showed four revolution period (Figure 26) being the contribution of the lower section predominant.
Finally the influence of the main rotor wake on the fuselage loads for the two different test conditions was investigated. For the case characterised by the tip vortices impinging on the leading edge of the horizontal tail plane (M_{WT}=0.031), the fuselage vertical load behaviour (Figure 27) showed higher fluctuating values respect the case (M_{WT}=0.059) characterised by the vortices moving far above the tail plane. Furthermore the lower speed case being more interested by the main rotor downwash effect presented for the vertical load a decrement of the mean value. At the same time the fuselage pitching moment coefficient presented a substantial increment of the fluctuation amplitude and a growth of the mean value indicating the achievement of the pitch up condition.

3.3. High speed

Within the high-speed case, at a free-stream and rotor Mach number of M_{WT}=0.259 and M_{MR}=0.617, model attitude of θ_F=1.1° the flow field behaviour at r/R=0.85 and 0.95 of the advancing rotor blade was investigated. The measurements suffered by lack of seeding concentration and by strong surface reflection blinding the region immediately close the surface. The instantaneous velocity fields showed an intense shock wave located on the blade upper surface (Figure 28) oscillating around the 37% of the blade chord.
For each single velocity field the azimuth angle position was measured. The analysis of the effective azimuth angles indicated a mean value equal at Ψ_{MR}=92.73° and a value of the standard deviation equal to 0.166°, confirming a real stable rotational speed of the main rotor. However the measured azimuth angle positions were apart up to a maximum of 0.74°, corresponding to a blade displacement of 16% of the blade chord. The shock location of the instantaneous velocity fields was investigated comparing the instantaneous u-component of the velocity extracted at fixed z locations (dashed line in Figure 28) for different azimuth positions. The results showed that the shock was separated by a distance equivalent to the 14% of the blade chord when the blade shift due to the different azimuth angles was equivalent to the 8.4% of the blade chord (Figure 29). The blade lag angle values contributed with a value of 0.4% and the flap and pitch blade angle contributions were negligible. The remaining 5% of distance was attributed to possible different blade deformations and to the intrinsic oscillation of the shock wave.
The ensemble average velocity field (Figure 30) was calculated re-positioning azimuthally all the instantaneous velocity fields such that all shocks were aligned with the shock corresponding to the mean azimuth angle (square bleu data in Figure 29).
The ensemble average data presented the same maximum speed respect the instantaneous velocity field but in concomitance of the shock the velocity step was slightly milder (Figure 31).

4. Concluding remarks

An extensive and successful measurement campaign was carried out on a full equipped and motorised helicopter model. Three component PIV measurements were performed on 37 different regions for two models configurations (isolated fuselage and full model) and four different flight conditions.
The influence of the main rotor wake on the fuselage was evaluated in terms of static and dynamic pressure distributions, horizontal tail plane loads, global fuselage loads and flow field analysis.
For the cruise/tail shake condition, the vortical structures in the wake region downstream the rotor hub were localised and their sources detected. The region below the fuselage for the full equipped model presented an increment of the strength of the detached vortices with a variation of their trajectories and an increment of the fuselage drag. Furthermore as consequence of the main rotor fuselage aerodynamic interaction the global loads on the fuselage presented a decrement of the fuselage vertical loads due to the downwash effect and a rising of the pitching moment.
The PIV measurement allowed selecting the appropriate flight condition for reaching the pitch up condition. The location and characteristics of the tip vortices impacting on the horizontal stabiliser were measured. The effects on the fuselage were measured and discussed. The fuselage results in terms of dynamic pressure and loads were in agreement with the conclusion drawn by the flow field measurements.
The compressibility effects occurring on the advancing blade were detected, and the location and strength of the shock wave was measured.
The results are now available to the GOAHEAD data base, providing a unique tool to the European helicopter industries and to the scientific community.
The GOAHEAD project has been a particularly successful example of cooperation between numerous European partners involved in instrumentation integration, measurements procedures, data exchange and data post processing procedures. The paper

presents just a small fraction of the gathered experimental data base.

5. Acknowledgements

This project was partially funded by the European Union within the 6th Framework European Research Programme, contract Nr. 516074.
The professional and personal commitment to the project by all the GOAHEAD partners and the DNW-LLF staff is gratefully acknowledged. The authors wish thanking dr. Antonio Pagano and dr. Berend van der Wall for their support and useful guide in the helicopter world.

References

[1] Heineck JT, Yamauchi GK, Wadcock AJ, Lourenco LM, Abrego AI, "Application of three-component PIV to a hovering rotor wake", AHS 56th Annual Forum, Virginia Beach, VA, USA, May 2-4, 2000.

[2] Martin PB, Pugliese GJ, Leishman JG "High resolution trailing vortex measurements in the wake of a hovering rotor", AHS 57th Annual Forum, Washington, DC, USA, May 9-11, 2001.

[3] Lee TE, Leishmann GJ, Ramasamy M, "Fluid Dynamics of Interacting Blade Tip Vortices With a Ground Plane", 64th Annual Forum of the American Helicopter Society, Montreal, Canada, April 29th – May 1st, 2008.

[4] Raffel M, Richard H, Ehrenfried K, van der Wall BG, Burley C, Beaumier P, McAlister K, Pengel K, "Recording and evaluation methods of PIV investigations on helicopter rotor model", Experiments in Fluids 36 pp 146-156, 2004.

[5] Le Pape A, Gatard J, Monnier JC, "Experimental Investigations of Rotor–Fuselage aerodynamic Interaction", Journal of American Helicopter Society 52 99, 2007.

[6] van der Wall BG, Richard H, "Analysis methodology for 3C-PIV data of rotary wing vortices", Experiments in Fluids vol.40, pp. 798–812, 2006.

[7] Pahlke KG, "The GOAHEAD Project", 33rd European Rotorcraft Forum, Kazan, Russia, September 11th-13th, 2007.

[8] Raffel M, De Gregorio F, Sheng W, Gibertini G, Seraudie A, de Groot K, van der Wall BG, "Generation of an advanced helicopter experimental aerodynamic database", 35th European Rotorcraft Forum, Hamburg, Germany, September 22nd – 25th, 2009.

[9] K. Kindler: "Dynamic stall on a fully equipped helicopter model", 36th European Rotorcraft Forum, Paris, France, September 7-9, 2010

[10] Barbagallo D, De Gregorio F, Tino N, "Pitch-Up Phenomenon characterisation by means of HW and PIV measurements Techniques", 26th European Rotorcraft Forum, The Hague, NL, September 26-29, 2000.

[11] de Waard PG, Trouvé M, Tail Shake vibration Objective comparison of aerodynamic configurations in a subjective environment", 55th American Helicopter Society Annual Forum, Montreal, Canada, 1999.

[12] Leishman JG, "Principle of Helicopter Aerodynamics", Cambridge University Press, 2000.

[13] F. De Gregorio, K. Pengel and K. Kindler: "Industrial Measurement Campaign on Fully Equipped Helicopter Model", 15th Int. Symp. on Applications of Laser Techniques to Fluid Mechanics, Lisbon, Portugal, 07-10 July, 2010

[14] B. Benoit, A.M. Dequin, K. Kamp, W. Von Gruenhagen, P.M. Basset and B. Gimonet, "HOST, a general helicopter simulation tool for Germany and France", In American Helicopter Society 56th Annual Forum, Virginia Beach, Virginia, USA, 2-4 May 2000. AHS.

[15] W. Sheng, "Data Post-Processor", GOAHEAD/WP4/UG/D4.1.4/A

Figure 1: Full equipped model

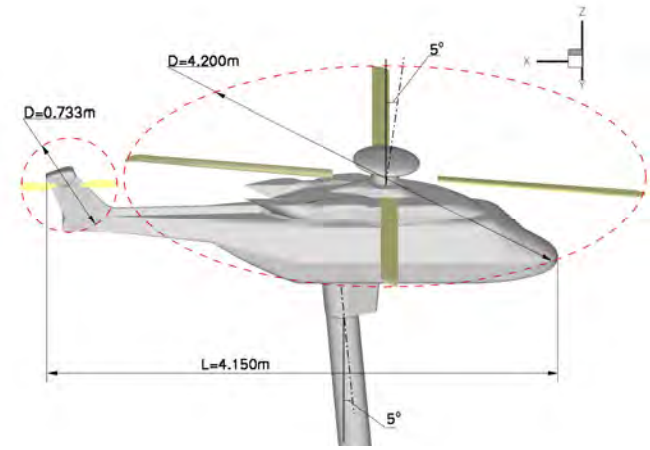

Figure 2:Overview of the helicopter model geometry

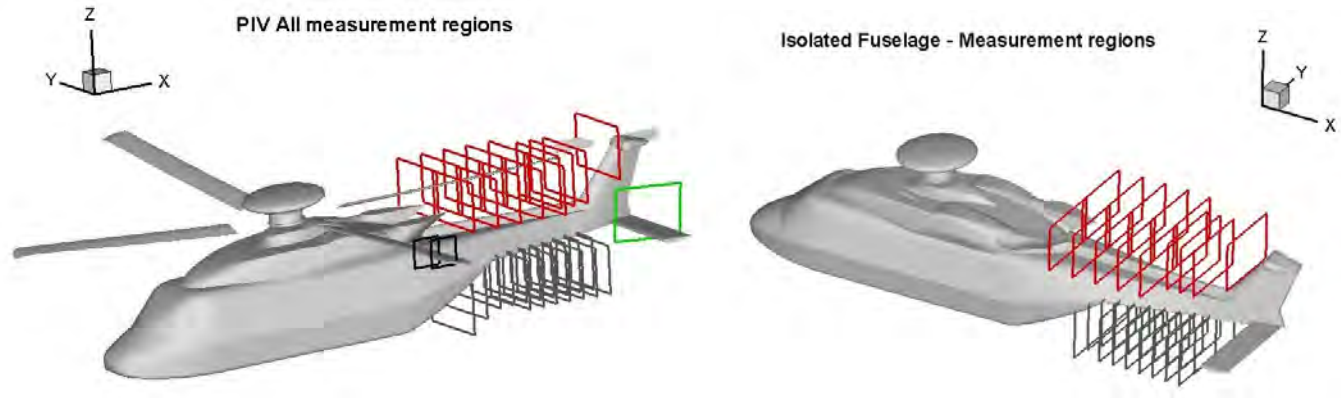

Figure 3: PIV measurement regions

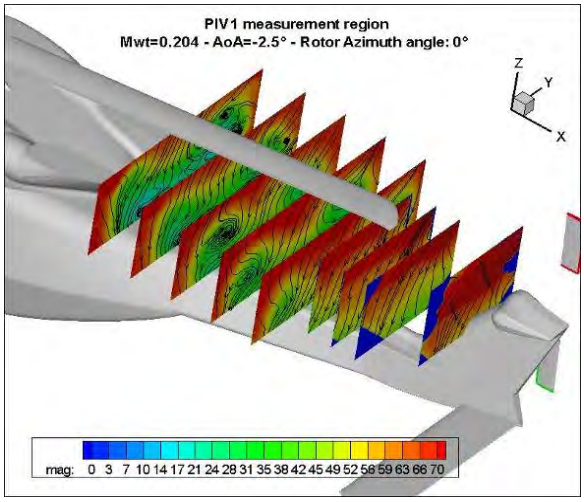

Figure 4: Flow field velocity magnitude for Ψ_{MR} =0°

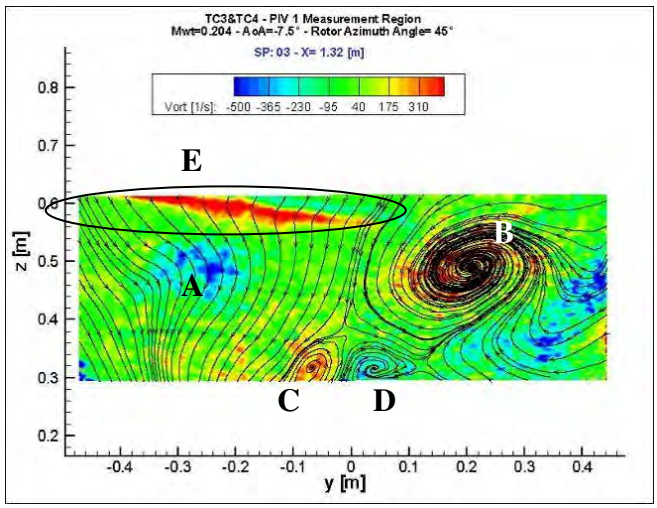

Figure 5: Flow vorticity map on the 3 scan plane at Ψ_{MR} =45°

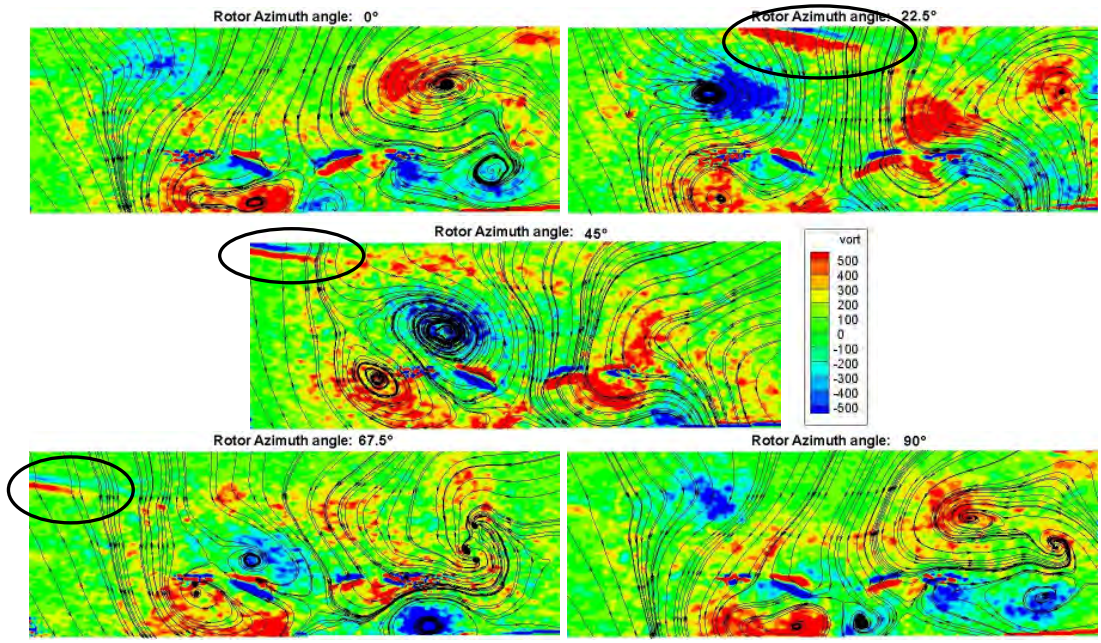

Figure 6: Flow vorticity map on the 1st scan plane for different azimuth angles

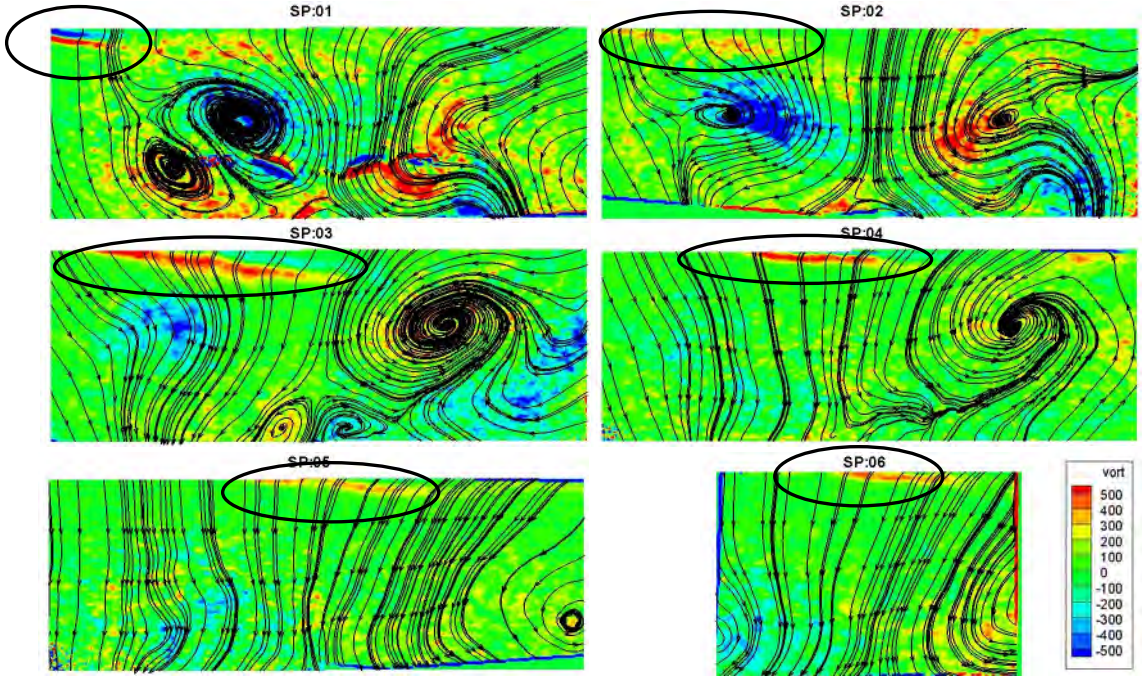

Figure 7: Flow vorticity map at Ψ_{MR} =45° for different scan planes

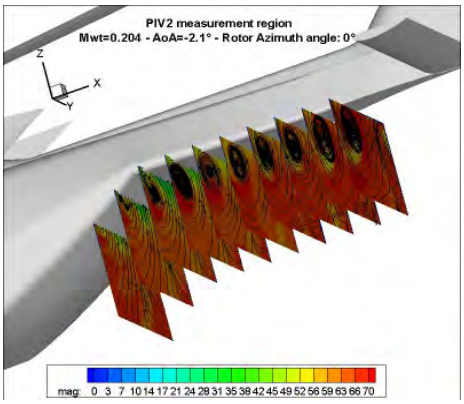

Figure 8: Velocity magnitude below the tail boom

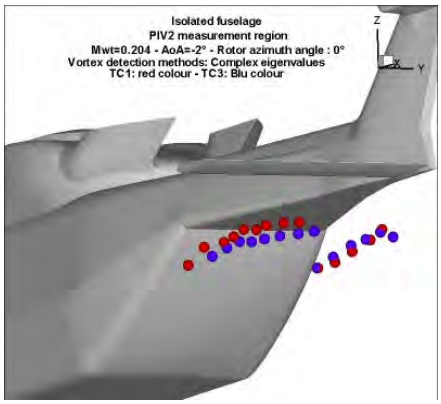

Figure 9: Vortex path isolated fuselage (red) full model (bleu)

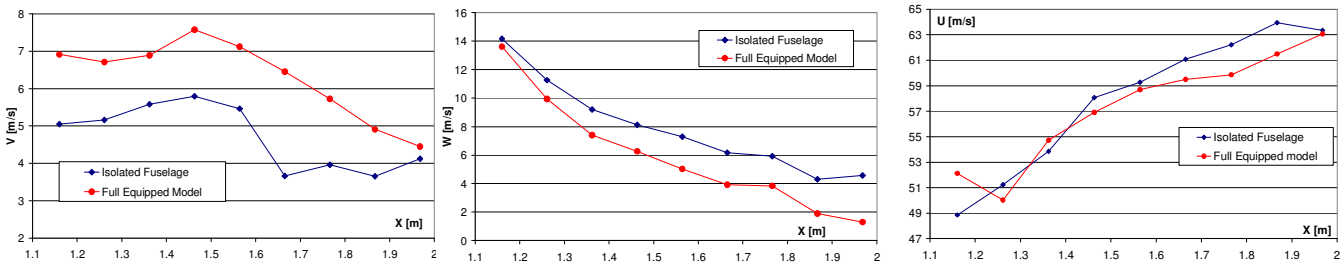

Figure 10: Mean velocity components comparison for isolated fuselage and full model

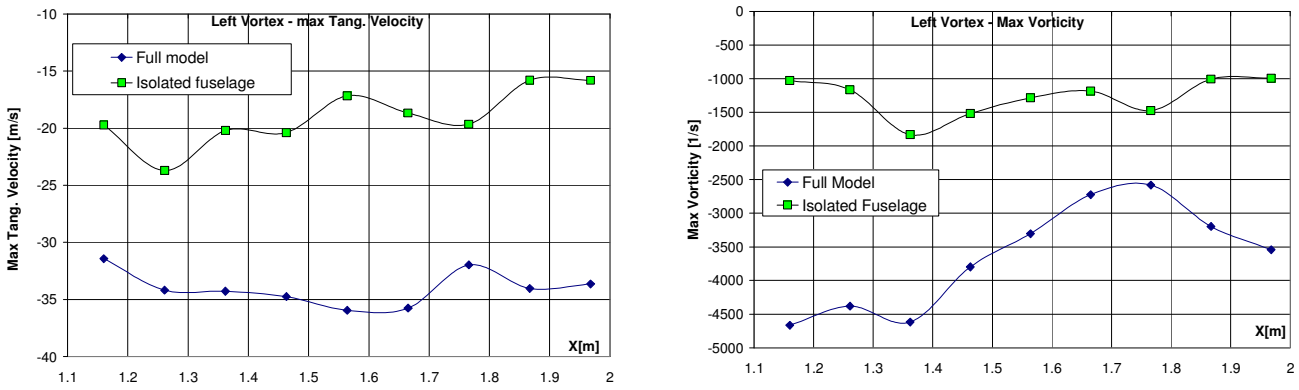

Figure 11:Vortex characteristics comparison between full model and isolated fuselage

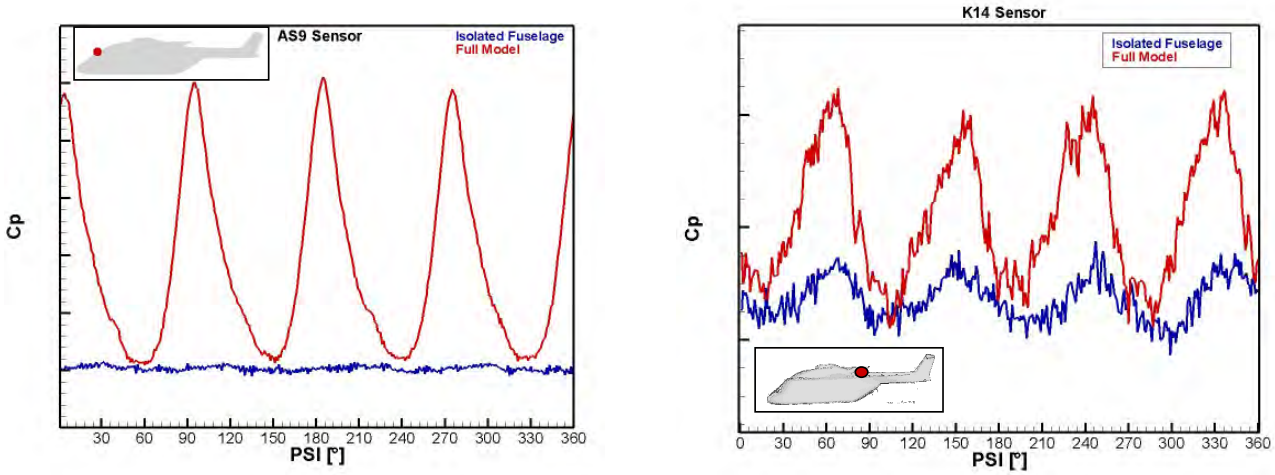

Figure 12: Dynamic pressure for isolated fuselage and full model configurations in cruise condition. Wind shield sensor (left) and tail boom sensor (right)

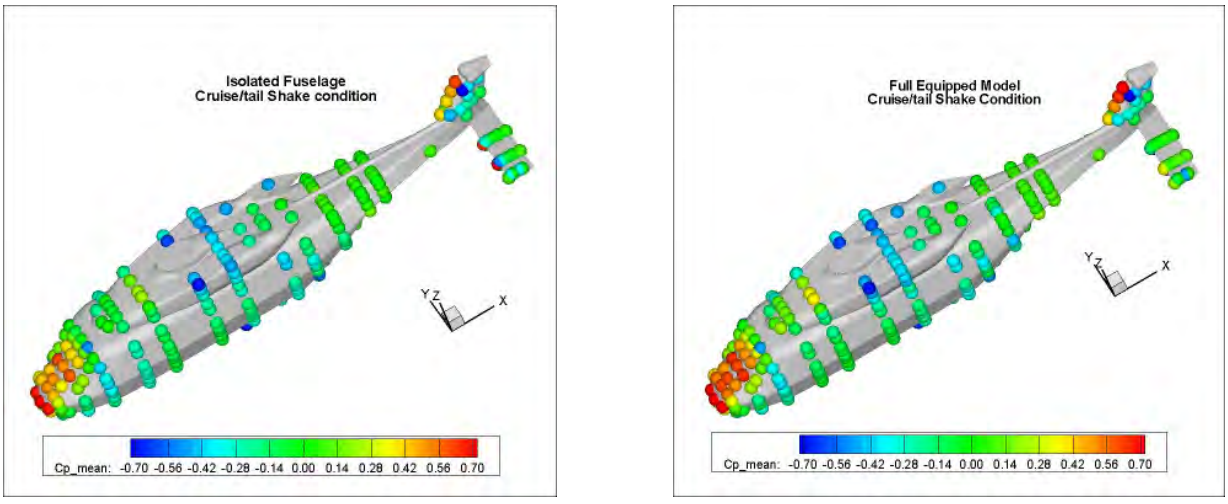

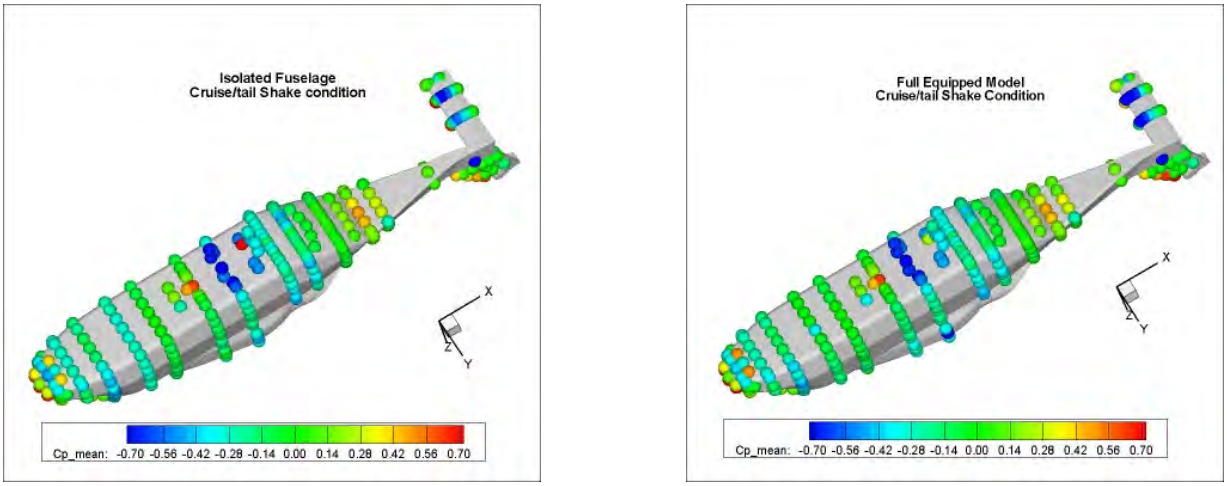

Figure 13: Mean pressure distribution for Isolated Fuselage (left) and Full Equipped Model (right).

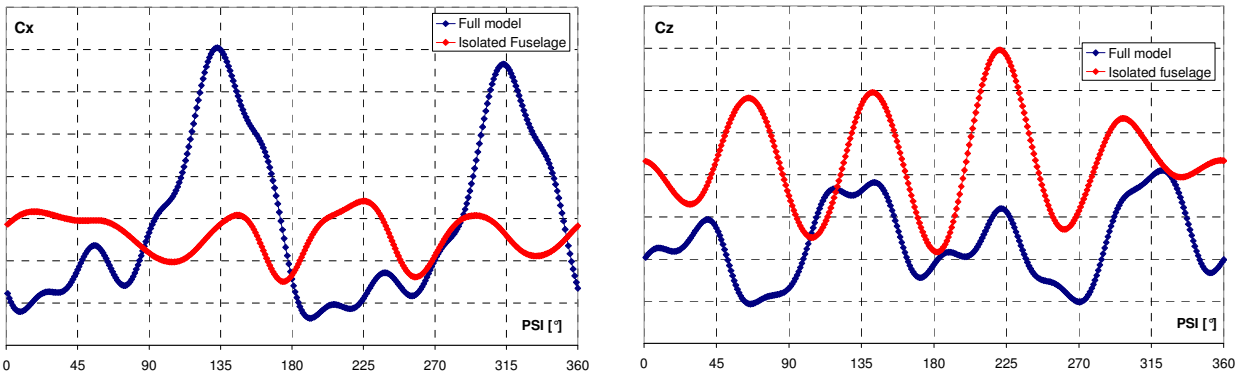

Figure 14: Fuselage vertical, and axial loads or isolated fuselage and full model configuration.

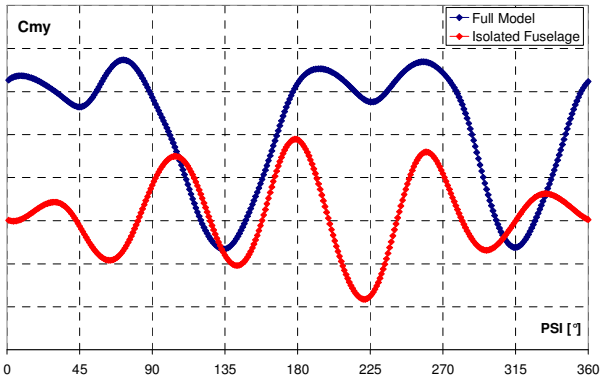

Figure 15: Fuselage pitching moment for isolated fuselage and full model configuration.

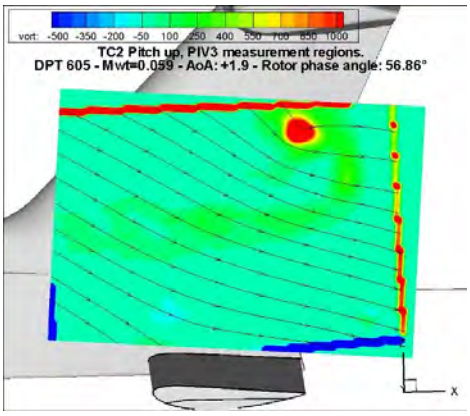

Figure 16: Vorticity map above horizontal tail plane

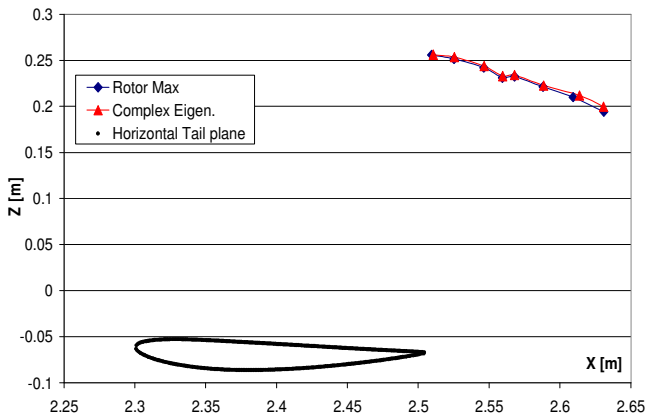

Figure 17: Vortex path above horizontal tail plane

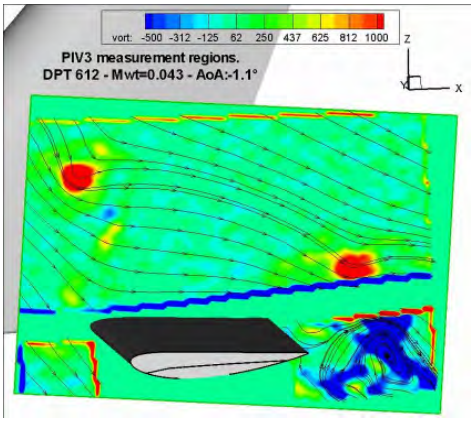

Figure 18: Vorticity map on horizontal plane (Ma=0.043)

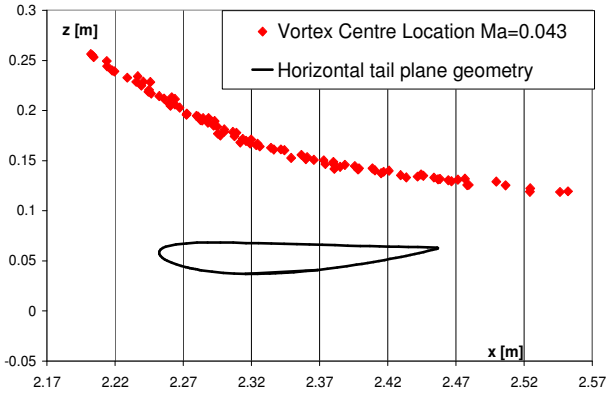

Figure 19: Vortex path for Ma=0.043.

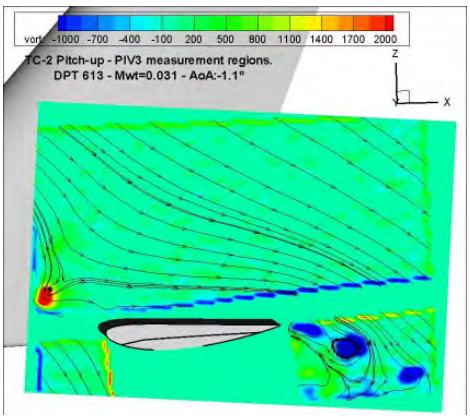

Figure 20: Vorticity map on horizontal plane (Ma=0.031)

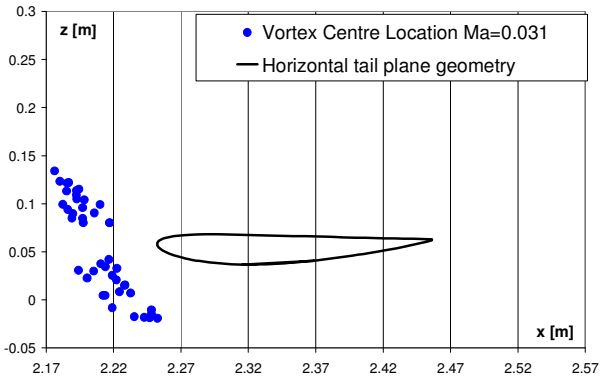

Figure 21: Vortex path for Ma=0.031

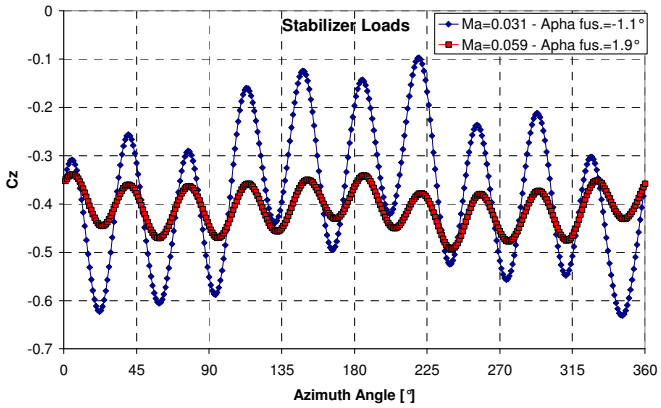

Figure 22: Vertical Loads on the horizontal stabilizer for different Mach and fuselage attitude

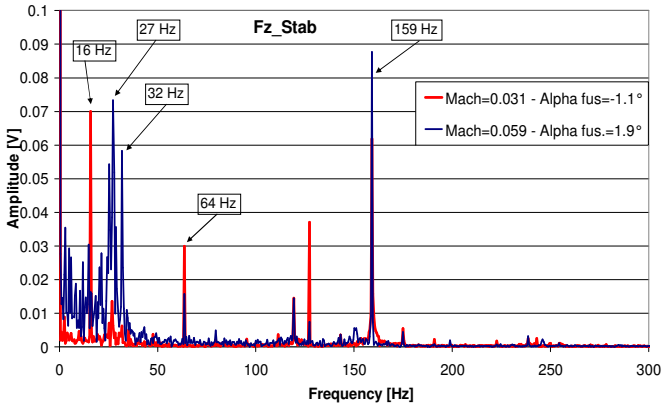

Figure 23: Spectrum of stabilizer loads

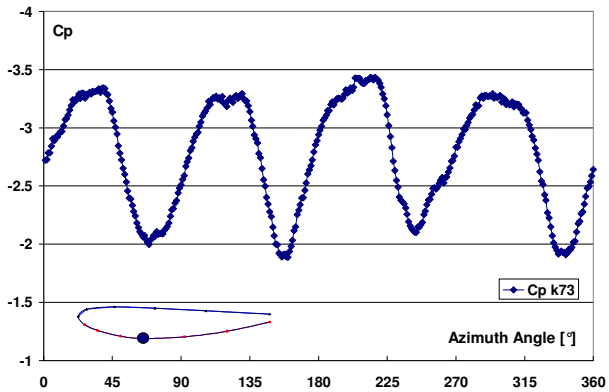

Figure 24: Horizontal tail plane lower surface pressure time history

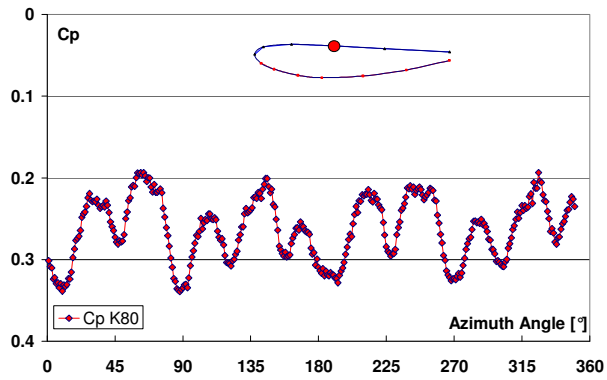

Figure 25: Horizontal tail plane upper surface pressure time history

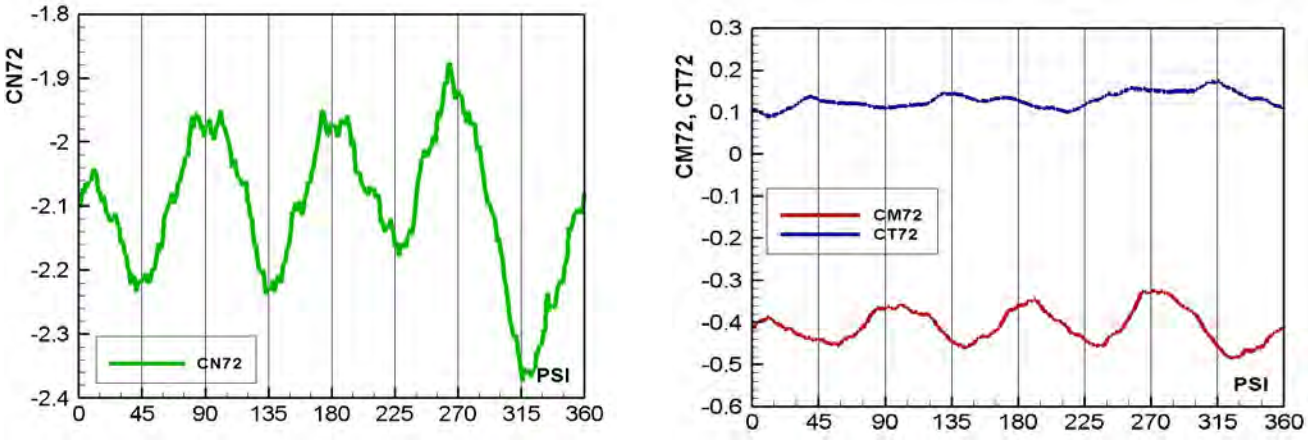

Figure 26: Horizontal tail plane pressure sectional load C_N (left), C_T and C_M (right).

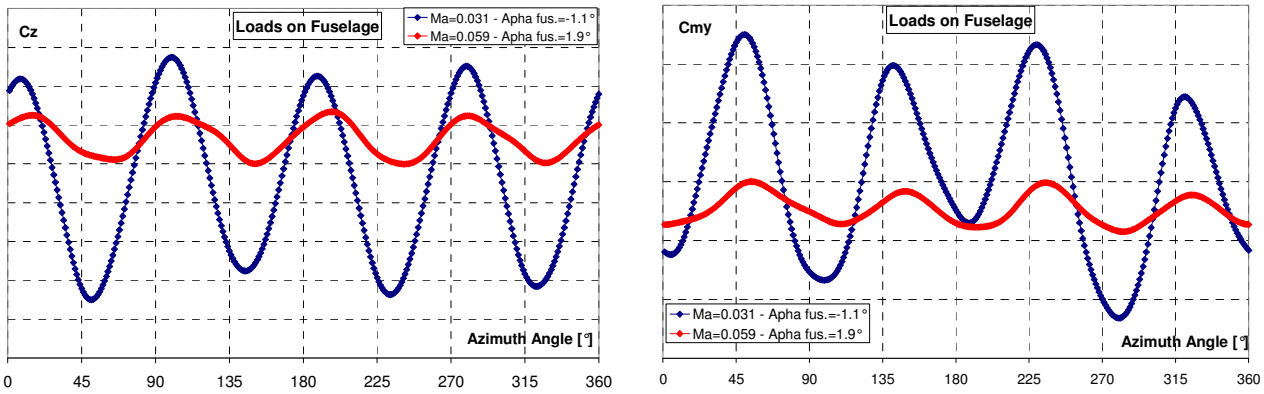

Figure 27: Fuselage Vertical load coefficient and pitching moment coefficient for M_{wt}=0.059 and M_{wt} =0.031.

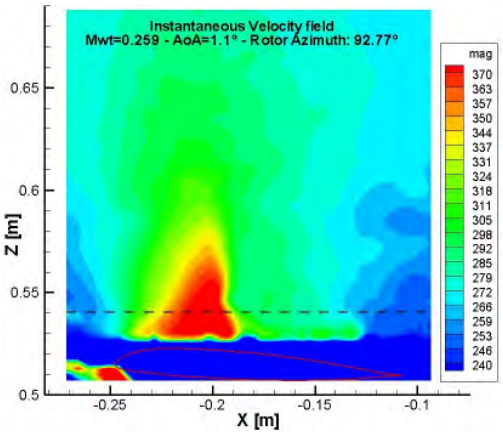

Figure 28: Instantaneous velocity field colour map.

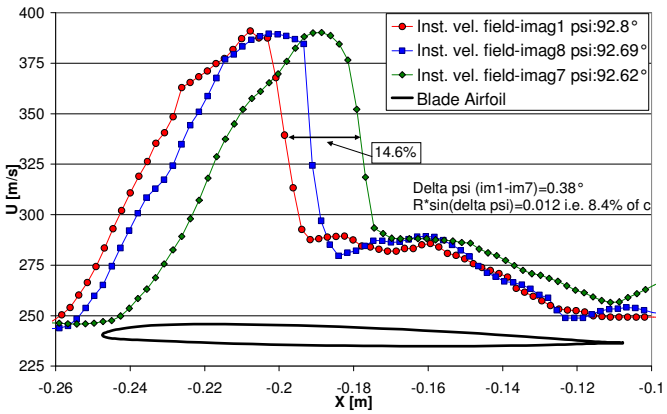

Figure 29: u velocity component for different azimuth angles

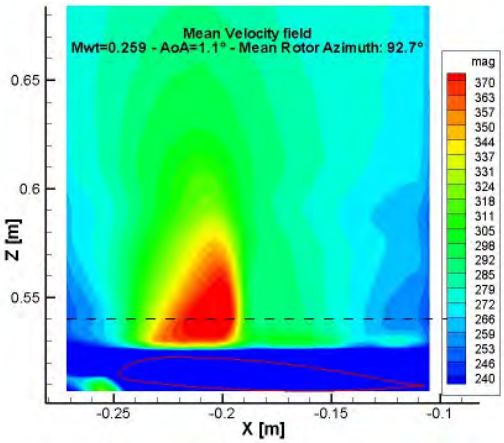

Figure 30: Mean velocity field colour map.

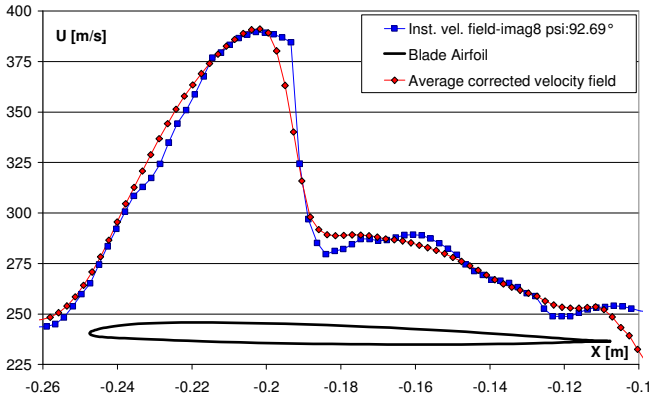

Figure 31: Mean and instantaneous u velocity component comparison.